Simplified Approach to Thermal Modeling of a Building Integrated Photovoltaic/thermal Façade

CCTC 2013 Paper Number 1569700499

H. Getu[1], A. S. Fung[1] and P. Dash[1]

[1] Department of Mechanical and Industrial Engineering, Ryerson University, Ontario, Canada

Abstract

The paper presents a theoretical study of the influence parameters such as air flow velocity and spacing between a photovoltaic panel and glass wall of photovoltaic/thermal (PV/T) integrated curtain wall. The outlet air temperature for different velocities and spacing between the PV panel and the glass wall was determined. For a given air velocity, increasing the spacing between the PV panel and the glass wall has the effect of decreasing the outlet temperature. Both the thermal and electrical energy were found to be higher in winter and fall seasons. From May to November, higher air velocities led to negative thermal energy recovered. Generally, in winter and fall seasons, increasing the air flow velocity increases the thermal and electrical efficiency. These results indicate that for given design parameters development and deployment of fan control strategies may be necessary to optimize the total energy production; both thermal and electrical.

Keywords: Building integrated photovoltaic/thermal (BIPV/T), solar energy, ventilated PV façade.

Résumé

Cet article présente une étude théorique de l'influence de paramètres comme la vitesse d'écoulement d'air et l'espace entre un panneau photovoltaïque et la paroi de verre du système photovoltaïque et thermique intégré dans le mur-rideau. La température de sortie d'air pour différentes vitesses et l'espace antre le panneau photovoltaïque et la paroi de verre ont été déterminés. Pour une vitesse d'air donnée, augmenter l'espace entre le panneau photovoltaïque et la paroi de verre a pour effet de diminuer la température de sortie. Les productions d'énergie thermique et électrique ont été trouvées plus élevées en hiver et en automne. De mai à novembre, une vitesse d'air plus importante entraine une énergie thermique récupérée négative. Généralement, en hiver et en automne, augmenter la vitesse d'écoulement d'air augmente l'efficacité thermique et électrique. Ces résultats indiquent que pour des paramètres de conception donnés, des stratégies de contrôle du ventilateur peuvent être nécessaires pour optimiser la production énergétique totale ; thermique et électrique.

1. Introduction

Solar energy is inexhaustible and import-independent resource that enhances energy security and sustainability, reduces pollution, lowers the cost of mitigating climate change, and keeps fossil fuel prices lower than otherwise [1]. Photovoltaic panels with a heat recovery capability, integrated into the building envelope replacing the elements of the roof or façade combine the possibility of cooling the PV panels, producing heat and electricity [2]. The heat recovered by fluid circulation behind the photovoltaic panels can be used for space and/or domestic water

heating. Various researchers have studied the possibilities of integrating PV panels into building façades and determined the energy performance [3-9]. Clarke et al. [3] conducted laboratory experiments and simulations of building façade integrated PV cells for a range of climatic conditions of the UK. Their analysis of the PV façade indicated an operational electric efficiency less than the peak published data, i.e. 12% compared to 15%. They also found that the utilization of thermal energy significantly increased the system efficiency by 33%, 44% and 57% for winter, spring and summer seasons, respectively. Mei et al. [4] used TRNSYS to conduct dynamic thermal modeling of an integrated ventilated PV façade/solar air collector system with experimental validation. They used the data collected from a PV panel integrated façade on the Mataro Library near Barcelona, Spain. They reported that 12% of heating energy can be saved using the pre-heated ventilation air for the building location in Barcelona in winter season. Charron and Athienitis [9] theoretically studied double-façades with integrated PV panels that can generate electricity and thermal energy. They found that when PV panels were installed in the middle of the cavity, i.e., between the outer glazing and inner glazing, the overall efficiency was increased by about 25%, however the electricity generated was lowered by 21%.

The above brief introduction clearly shows that ventilated façades with integrated PV are viable options that combine the advantages of producing electricity and generating thermal energy. The present work examined the influence of different design parameters of PV/T integrated wall for the Greater Toronto Area (GTA) climatic conditions.

2. System description

Fig. 1 shows the schematic of the system investigated, air flowing behind the PV panels as a thermal energy recovery medium. The dimensions of the PV/T were selected arbitrarily but within the limit of the height a wall of typical house (2.5 m) and the width represents approximately 50% of the width of the wall of a room with a floor area of approximately 50 m^2 in size.

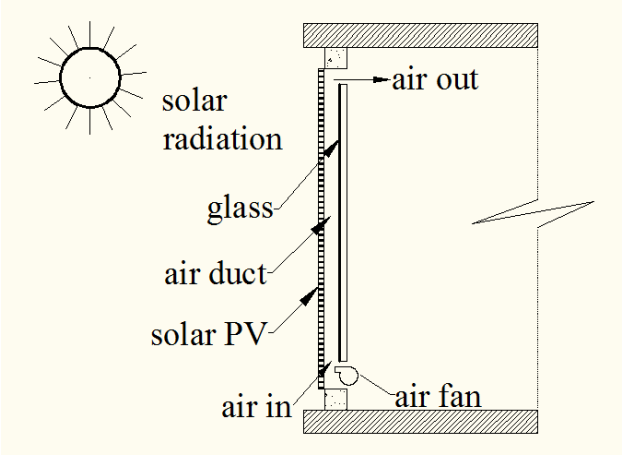

Figure 1. Schematic of the façade integrated PV/T.

3. Mathematical model

Energy balance equations were used to determine the outlet temperature of the air from the duct. The following assumptions were made in writing the energy balance equations:

(a) 1-D steady state heat transfer conditions,

(b) The heat capacity of photovoltaic/thermal (PV/T) system was considered negligible in comparison to the heat capacity of the air,
(c) The specific heat capacity of air, C_p, remains constant, i.e. does not change with temperature change in the gap between the PV panel and the glazing,
(d) 4 m wide 2.5 m high PV panels were assumed.

For the PV cell:

$$\alpha_{pv}\ 1-\eta_{el}\ \ I_r b dx = U_{pv}\ \ T_{pv}-T_a\ \ b dx + h_{cpv}\ \ T_c - T_f\ \ b dx + h_{rpv}\ \ T_{pv}-T_g\ \ b dx \quad (1)$$

For the air stream flowing in the duct:

$$m_a C_p \frac{dT_f}{dx} dx = h_{cpv}\ \ T_{pv}-T_f\ \ b dx + h_{cg}(T_g - T_f) b dx \quad (2)$$

For the inside surface of the glass:

$$I_r \tau_{pv} \alpha_g = h_{rgs}(T_g - T_{pv}) + h_{cg}\ \ T_g - T_f\ \ + U_g\ \ T_g - T_i \quad (3)$$

The above equations can be combined and solved to obtain the outlet fluid temperature, T_f mean temperature, T_m the PV panel temperature and T_{pv}. In this study, a PV system with the following parameters and assumptions was considered (Table 1).

Table 1: Material specifications, model assumptions and inputs used.

variable	value	variable	value
α_{pv}	0.9	h_i	2.8
α_g	0.06	m_a	ρvbD
δ_{pv}	0.05	h_w	$2.8+3v_a$
L	2.5 m	η_{el}	0.15
C_p	1007 J/KgK	ρ	1.164 kg/m^3
b	4 m	T_{in}	22 °C
α_{pv}	0.05	R_g	0.4
v	varies	D	10 mm, 40mm, 80 mm

Data of monthly average daily global irradiation, wind velocity and temperature values obtained from Meteonorm meteorological database version 7 for GTA (latitude=43.7°N, longitude=-79.2°E, elevation=157m) were used. The Perez sky model was used to transform Meteonorm data to incident irradiance on the façade. The convective heat transfer coefficients in the air gap for the PV side, h_{cpv}, were calculated by assuming the heat transfer process to combine both forced and natural convection, and laminar and turbulent flow. For such mixed flow conditions with lower air flow velocities (< 0.5 m/s) an appropriate mixture flow conditions must be used [4]. Nusselt number, described by the following equations [10], which is useful for mixed flow conditions (< 0.5 m/s) [4] was used to determine the convective heat transfer coefficients.

$$\overline{Nu} = \sqrt{\overline{Nu}_{lam}^2 + \overline{Nu}_{turb}^2} \quad (4)$$

where $\overline{Nu}_{lam} = 0.644\sqrt{Re}\sqrt[3]{Pr}$ (5)

$$\overline{Nu}_{tur} = \frac{0.037 Pr Re^{0.8}}{1+2.44Re^{-0.1}\ \ Pr^{2/3}-1} \quad (6)$$

$$Re = \sqrt{Re_{forc}^2 + Re_{free}^2} \quad (7)$$

$$Re_{forc} = \frac{vH}{v}, Re_{free} = \sqrt{\frac{Gr}{2.5}} \quad (8)$$

$$h_{cpv} = \frac{\overline{Nu}\kappa}{D} \quad (9)$$

where $\overline{Nu}$ is Nusselt number for mixed flow condition, Re is Reynolds number, v is the air velocity, H is hydraulic diameter, Gr is Grashof number, Pr is the Prandtl number, κ is the thermal conductivity of air and D is the spacing between the PV panel and the glass wall. Subscripts *forc* and *free* denote forced and free convection.

The Reynolds number for free convection requires determination of the Grashof number, which in turn requires the knowledge of the temperature of the PV panel and the ambient temperature. In this work, varying PV panel temperatures were assumed (0°C-70°C) to determine the convective heat transfer coefficients, h_{cpv}, for different velocities. The h_{cpv} values increased with increasing velocities, but showed slight changes over the range of PV temperatures considered for a given velocity and air gap depth (Fig. 2). Therefore an average value of the convective heat transfer coefficient was used for a given velocity and air gap depth. Table 2 gives the average values of the convective heat transfer coefficients used for different velocities and spacing between the PV and the glazing (D).

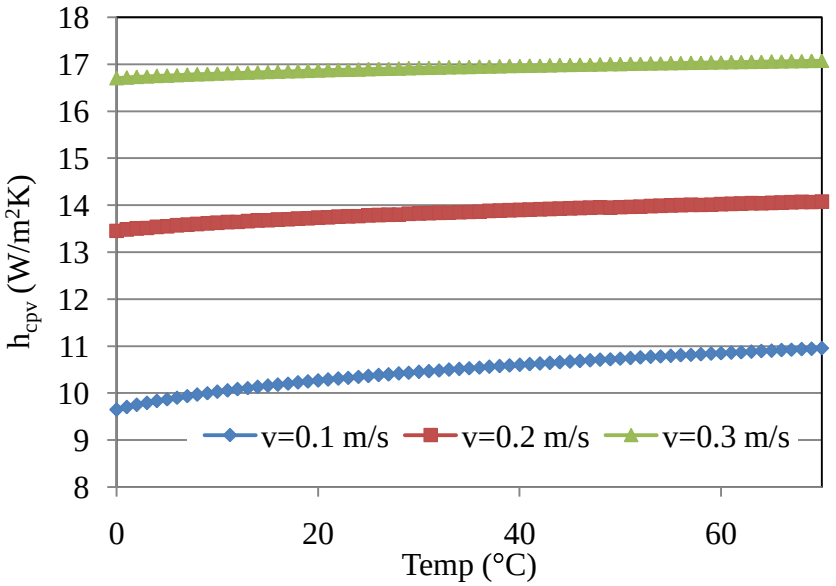

Figure 2. Variation of convective heat transfer coefficient for different PV temperature and various velocities, D=40 mm.

Table 2 Convective heat transfer coefficient for different velocities and air gap depths, D.

h_{cpv}(W/m^{2}K)																
	Depth=10mm					Depth=40mm					Depth=80mm					
	Velocity (m/s)					Velocity (m/s)					Velocity (m/s)					
	0.01	0.05	0.1	0.2	0.3	0.01	0.05	0.1	0.2	0.3	0.01	0.05	0.1	0.2	0.3	
h_{cpv}	32.2	32.4	33.1	35.4	38.4	8.5	9.2	10.5	14	17	4.1	5.2	6.8	9.8	12.3	

4. Results and discussion

4.1 Outlet and PV temperatures

Fig. 3 shows the average monthly variation of the outlet and PV panel temperatures. It is observed that the temperature difference ($\Delta T=T_f-T_a$) is higher in winter and fall seasons. This is because the winter sun comes at low angles for higher altitude locations such as GTA.

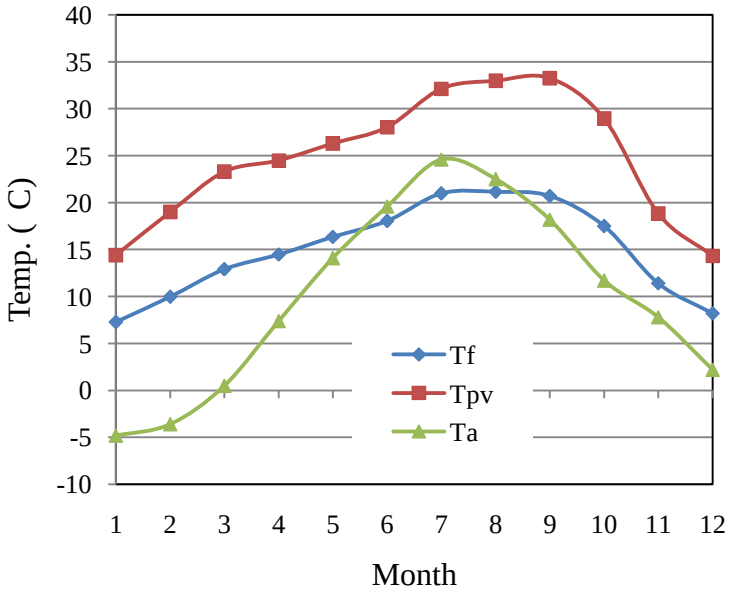

Figure 3. Average monthly variation of the outlet air (T_f), PV (T_{pv}) and inlet temperatures (T_a). v=0.1m/s, b=4m, D=80 mm.

Fig. 4 shows variation of the monthly average outlet temperature, T_f, for different air velocities. Generally, as observed from Fig. 6, the outlet temperature decreases as the air flow rate increases. This is in agreement with the results of Charron and Athienitis [9] who reported that higher air velocities lead to lower air temperature in the air gap because the heat removal factor is increased. This is clearly seen from the decreasing PV panel temperature with increasing air velocity (Fig. 5), which may also lead to higher electrical efficiency.

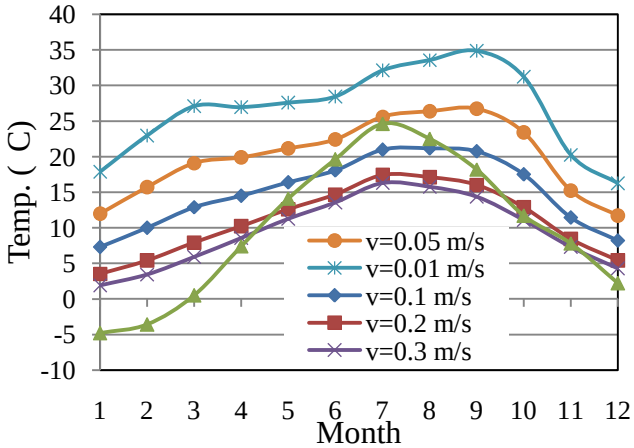

Figure 4. Average monthly variation of the outlet air temperature, T_f, for various velocities.b=4m, D=80 mm.

In spring and summer, it is observed that the outlet temperature shows lower increase ($\Delta T=T_f - T_a$) as compared to the outlet temperature in winter. The reason is that the available incident solar radiation during these seasons is equal or slightly less than that of the winter and fall seasons (Table 3). It is noted that the incident radiation is lower in November and December.

Table 3 Incident solar radiation on the surface of the PV/T integrated curtain wall.

Month	Jan	Feb	Mar	Apr	May	Jun	Jul	Aug	Sep	Oct	Nov	Dec
I_r (W/m^2)	108	133	146	129	117	108	117	129	146	142	92	83

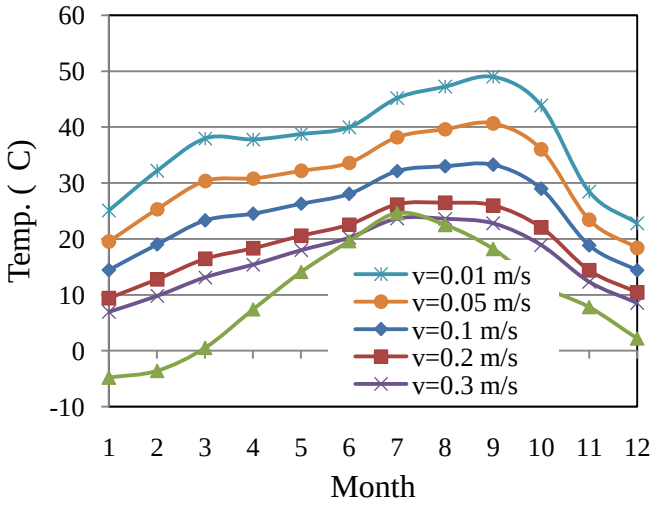

Figure 5. Average monthly variation of the PV temperature, T_{pv}.b=4m, D=80 mm.

Fig. 6 shows variation of the outlet temperature, T_f, for different air gap depths, D, between the PV and the glass for 0.1 m/s air velocity. Increasing the air gap depths (D) between the PV and the glass results in higher outlet temperatures.This is because increasing air gap depth increases the air mass flow rate ($m_a=\rho vbD$)leading to higher the outlet temperature.

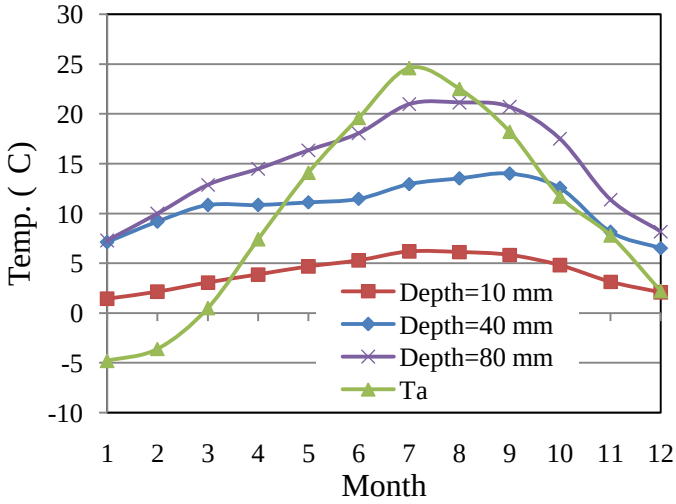

Figure 6. Average monthly variation of the outlet temperature, T_f, for various air gap depths, D.b=4m, v=0.1m/s.

4.2 Thermal and electrical energy

Thermal (Q_t) and electrical (Q_e) energy were calculated using Eq. 10 and Eq. 11, respectively.

$$Q_t = m_a C_p \ T_f - T_a \quad (10)$$

$$Q_e = \eta_{pv} A I_r \quad (11)$$

where $\eta_{pv} = \eta_{Tref} \ 1 - \beta_{ref} \ T_{pv} - T_{ref}$ (12)

is the PV electrical efficiency, A is the PV surface area, η_{Tref} is the PV module's electrical efficiency at reference temperature, T_{ref} (25°C) and at solar radiation of 1000 W/m^2, β_{ref} is the PV module's temperature coefficient. A 15% value was assumed for η_{Tref}. β_{ref} was calculated using Eq. 13 [11].

$$\beta_{ref} = \frac{1}{T_o - T_{ref}} \quad (13)$$

where T_o is the temperature at which the PV module's electrical efficiency drops to zero [12]. In this work, this temperature was assumed to be 270 °C [13]. Using Eq. 13, the value of β_{ref} was calculated to be 0.004°C^{-1}, which is in agreement with the value given in [11]. Generally, the thermal energy recovered was found to be higher in winter (Fig. 7, Table 4).The peak electrical energy obtained was in March and October corresponding to the highest incident solar radiation available (Table 3).

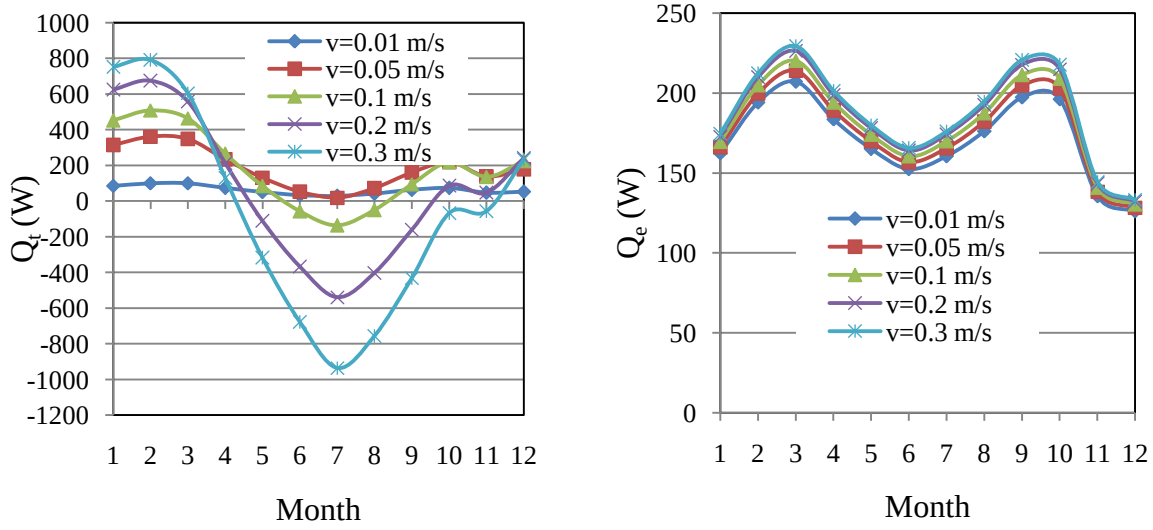

Figure 7. Thermal (a) and electrical (b) energy for different velocities; *D*=80mm.

Generally, the higher the air velocity the higher the thermal energy recovered. From April to August, higher air velocities lead to negative thermal energy recovered. This is because of lower radiation received because the sun comes at high angles. During these months, the circulating air has a cooling effect leading to negative thermal energy production.

Table 4: Thermal energy recovered for different velocities at a given air gap (*D*) values.

Q_t (W)															
	Depth=10mm					Depth=40mm					Depth=80mm				
	Velocity (m/s)					Velocity (m/s)					Velocity (m/s)				
	0.01	0.05	0.1	0.2	0.3	0.01	0.05	0.1	0.2	0.3	0.01	0.05	0.1	0.2	0.3
Jan	3	15	29	58	85	26	122	223	368	485	85	314	452	624	752
Feb	3	14	27	53	77	28	133	239	380	488	99	361	508	674	790
Mar	1	6	12	23	31	24	112	193	277	327	99	348	464	557	605
Apr	-2	-8	-16	-35	-56	11	47	64	27	-37	73	233	265	211	129
May	-4	-22	-44	-91	-140	-1	-13	-56	-209	-381	50	132	85	-111	-318
Jun	-7	-33	-67	-137	-210	-10	-62	-152	-399	-660	33	52	-58	-368	-677
Jul	-9	-43	-86	-176	-269	-16	-93	-218	-540	-875	28	19	-136	-539	-935
Aug	-8	-38	-77	-156	-241	-11	-67	-168	-448	-746	41	72	-51	-404	-757
Sep	-6	-29	-58	-119	-184	-2	-21	-79	-279	-504	62	159	94	-162	-432
Oct	-3	-16	-32	-67	-105	7	25	16	-83	-208	73	219	217	86	-68
Nov	-2	-11	-22	-45	-71	4	14	7	-61	-145	47	139	135	46	-58
Dec	0	0	-1	-2	-5	11	50	81	98	97	52	178	224	240	234

For the smallest air gap investigated the increase in velocity from 0.01 m/s to 0.2 m/s did not lead to increase in the electrical energy produced (Table 5), indicating the heat removal was not efficient enough. When the air gap depth was either 40 mm or 80 mm, every increase in the air velocity resulted in increased electrical energy produced.

Table 5: Electrical energy recovered for different velocities at a given air gap (*D*) values.

Q_e (W)															
Month	Depth=10mm					Depth=40mm					Depth=80mm				
	Velocity (m/s)					Velocity (m/s)					Velocity (m/s)				
	0.01	0.05	0.1	0.2	0.3	0.01	0.05	0.1	0.2	0.3	0.01	0.05	0.1	0.2	0.3
Jan	177	177	177	177	178	169	170	171	173	174	162	166	169	173	174
Feb	217	217	217	217	218	205	206	208	211	212	194	200	205	210	212
Mar	236	236	236	236	237	221	223	225	228	231	207	214	220	226	229
Apr	208	208	208	208	209	196	197	199	202	204	184	189	194	199	201
May	187	187	187	187	188	177	178	179	182	184	165	170	174	178	180
Jun	173	173	173	173	173	164	165	166	169	170	153	157	160	164	166
Jul	185	185	185	185	186	174	175	177	180	182	161	166	170	174	176
Aug	205	205	205	205	206	192	193	195	199	201	176	182	187	193	195
Sep	231	231	232	232	233	216	217	220	224	227	197	205	211	218	221
Oct	227	227	227	227	228	212	214	216	220	222	196	203	209	215	218
Nov	148	148	148	148	149	142	143	144	145	146	136	138	141	143	145
Dec	136	136	136	136	136	131	131	132	133	134	126	128	130	132	133

4.3 PV electrical efficiency

The PV electrical efficiency was calculated using Eq. 12 [11]. In most cases, the PV's electrical efficiency was found to be slightly more than the assumed 15%value for winter and fall seasons. This is probably because of the low PV temperature for this season, which is lower than the test temperature. For low air flow velocity (0.1 m/s) the PV temperature was above the test temperature, 25°C, (Fig. 5). It is seen that the PV's efficiency drops below 15%. These values are shown in bold italics in Table 6. This is in agreement with the results of Clarke et al. [3] who conducted laboratory experiments and reported an operational electrical efficiency less than the peak published data, 12% compared to 15%, for cell temperatures above 25°C.

4.3.1 Effect of changing air velocity at constant air gap depth

Table 6 shows that for a given air gap depth, *D*, increasing the air velocity increases the PV's electrical efficiency. This is because of higher air flow rates that lead to lower PV temperatures. It is noted that for the smallest air gap, i.e., 10mm, the increase in PV's efficiency with increasing air velocity is small; and for the largest air gap depth (80 mm), the increase in the PV's efficiency is around7% (Fig. 8).

Table6: PV efficiency for different velocities at a given air gap depth (*D*) values.

η_{pv}(%)															
	Depth=10mm					Depth=40mm					Depth=80mm				
	Velocity (m/s)					Velocity (m/s)					Velocity (m/s)				
	0.01	0.05	0.1	0.2	0.3	0.01	0.05	0.1	0.2	0.3	0.01	0.05	0.1	0.2	0.3
Jan	16.4	16.4	16.4	16.4	16.4	15.6	15.7	15.8	16.0	16.1	15.0	15.3	15.7	16.0	16.1
Feb	16.3	16.3	16.3	16.3	16.3	15.4	15.5	15.6	15.8	15.9	***14.6***	15.0	15.4	15.8	15.9
Mar	16.2	16.2	16.2	16.2	16.2	15.2	15.3	15.4	15.7	15.8	***14.2***	***14.7***	15.1	15.5	15.7
Apr	16.1	16.1	16.1	16.1	16.2	15.2	15.3	15.4	15.7	15.8	***14.2***	***14.6***	15.0	15.4	15.6
May	16.0	16.0	16.0	16.0	16.1	15.2	15.2	15.4	15.6	15.8	***14.2***	***14.6***	***14.9***	15.3	15.4
Jun	15.9	15.9	16.0	16.0	16.0	15.1	15.2	15.3	15.6	15.7	***14.1***	***14.5***	***14.8***	15.2	15.3
Jul	15.8	15.8	15.9	15.9	15.9	***14.9***	15.0	15.2	15.5	15.6	***13.8***	***14.2***	***14.6***	***14.9***	15.1
Aug	15.8	15.8	15.9	15.9	15.9	***14.9***	15.0	15.1	15.4	15.6	***13.6***	***14.1***	***14.5***	***14.9***	15.1
Sep	15.9	15.9	15.9	15.9	16.0	***14.8***	14.9	15.1	15.4	15.6	***13.5***	***14.0***	***14.5***	***14.9***	15.1
Oct	16.0	16.0	16.0	16.0	16.1	15.0	15.1	15.2	15.5	15.7	***13.9***	***14.3***	***14.8***	15.2	15.4
Nov	16.2	16.2	16.2	16.2	16.2	15.5	15.6	15.7	15.9	16.0	***14.8***	15.1	15.4	15.7	15.8
Dec	16.3	16.3	16.3	16.3	16.3	15.7	15.8	15.9	16.0	16.1	15.1	15.4	15.7	15.9	16.0

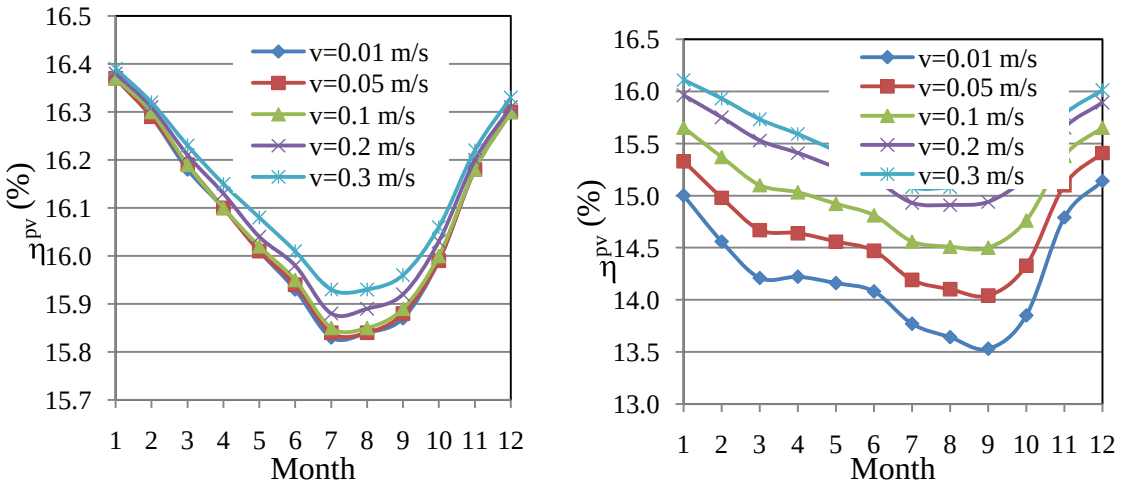

Figure 8. Variation of PV electrical efficiency for various air velocities in the duct for constant velocity. b=4m, (a) air gap depth=10mm, (b) air gap depth=80mm.

4.3.2 Effect of changing the air gap depth at constant air velocity

Table 7 gives the effect of varying the air gap depth on the PV's electrical efficiency at a constant air velocity. Increasing the air gap depth from 10 mm either to 40 mm or 80 mm for a given air velocity reduced the PV's electrical efficiency (Table 7, Fig 9a). This because of the decreasing convective heat transfer coefficient, which is indirectly proportional to the air gap depth, *D,* according to Eq. 9. To improve the PV's electrical efficiency, it is necessary increase the air gap depth with increasing air velocity. For example, for 80 mm air gap depth, increasing the air velocity from 0.1 m/s to 0.4 m/s increased the PV's electrical efficiency. This is shown in Table 7 (bold italics) and Fig. 9b.

Table7: PV electrical efficiency for different depths at a given air velocity.

η_{pv} (%)										
	v=0.1m/s			*v*=0.2m/s			*v*=0.3m/s			*v*=0.4m/s
	Depth			Depth			Depth			Depth
	10mm	40mm	80mm	10mm	40mm	80mm	10mm	40mm	80mm	80mm
Jan	16.4	15.8	***15.7***	16.4	16.0	16.0	16.4	16.1	16.1	***16.4***
Feb	16.3	15.6	***15.4***	16.3	15.8	15.8	16.3	15.9	15.9	***16.3***
Mar	16.2	15.4	***15.1***	16.2	15.7	15.5	16.2	15.8	15.7	***16.0***
Apr	16.1	15.4	***15.0***	16.1	15.7	15.4	16.2	15.8	15.6	***15.8***
May	16.0	15.4	***14.9***	16.0	15.6	15.3	16.1	15.8	15.4	***15.5***
Jun	16.0	15.3	***14.8***	16.0	15.6	15.2	16.0	15.7	15.3	***15.3***
Jul	15.9	15.2	***14.6***	15.9	15.5	14.9	15.9	15.6	15.1	***15.1***
Aug	15.9	15.1	***14.5***	15.9	15.4	14.9	15.9	15.6	15.1	***15.1***
Sep	15.9	15.1	***14.5***	15.9	15.4	14.9	16.0	15.6	15.1	***15.3***
Oct	16.0	15.2	***14.8***	16.0	15.5	15.2	16.1	15.7	15.4	***15.6***
Nov	16.2	15.7	***15.4***	16.2	15.9	15.7	16.2	16.0	15.8	***15.9***
Dec	16.3	15.9	***15.7***	16.3	16.0	15.9	16.3	16.1	16.0	***16.2***

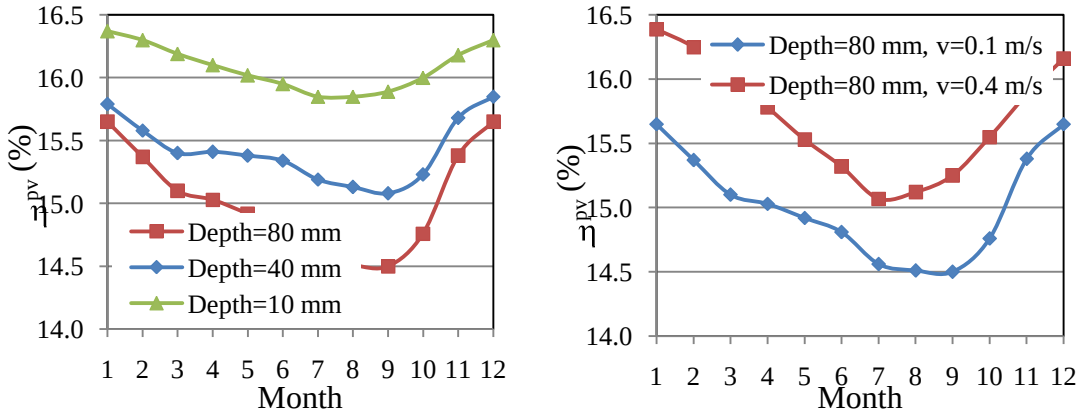

(a) (b)

Figure 9. (a) Variation of PV electrical efficiency for different gap depths in the duct. b=4m, v=0.2m/s and (b) increase in PV efficiency for increasing air velocity from 0.1 m/s to 0.4m/s, b=4m, gap depth =80 mm.

4.4 Thermal efficiency

The thermal efficiency was calculated using Eq. 14 [14].

$$\eta_t = \frac{Q_t}{AI_r} \tag{14}$$

where A is the PV area and I_r is the incident solar radiation and Q_t is the extracted thermal energy calculated using Eq. 10 [14]. Generally, in winter and fall, when the sun is low (Fig. 5), higher incident solar radiation is received by the PV panels, which leads to higher thermal energy recovered.

4.4.1 Effect of changing air velocity at constant air gap depth, *D*

Table 8 shows the effect of changing air velocity on the thermal efficiency for a given air gap depth. Generally, as expected, in winter, increasing the air velocity increases the thermal

efficiency (Fig. 10). In spring and summer, increasing the air velocity reduced the thermal efficiency. This is because of relatively low solar radiation received by the PV panels due to the sun's positions during these seasons. The circulating air behind the PV panel may even have a cooling effect leading to negative thermal energy (Fig. 10). As there is no need for heating in spring and summer this may actually be desirable.

Table8: Thermal efficiency for different velocities at a given air gap depth, *D.*

η_t (%)															
Month	Depth=10mm					Depth=40mm					Depth=80mm				
	Velocity (m/s)					Velocity (m/s)					Velocity (m/s)				
	0.01	0.05	0.1	0.2	0.3	0.01	0.05	0.1	0.2	0.3	0.01	0.05	0.1	0.2	0.3
Jan	0.3	1	3	5	8	2	11	21	34	45	8	29	42	58	69
Feb	0.2	1	2	4	6	2	10	18	29	37	7	27	38	51	59
Mar	0.1	0.4	1	2	2	2	8	13	19	22	7	24	32	38	42
Apr	-0.1	-1	-1	-3	-4	1	4	5	2	-3	6	18	21	16	10
May	-0.4	-2	-4	-8	-12	0	-1	-5	-18	-33	4	11	7	-9	-27
Jun	-0.6	-3	-6	-13	-19	-1	-6	-14	-37	-61	3	5	-5	-34	-63
Jul	-0.7	-4	-7	-15	-23	-1	-8	-19	-46	-75	2	2	-12	-46	-80
Aug	-0.6	-3	-6	-12	-19	-1	-5	-13	-35	-58	3	6	-4	-31	-59
Sep	-0.4	-2	-4	-8	-13	0	-1	-5	-19	-35	4	11	6	-11	-30
Oct	-0.2	-1	-2	-5	-7	1	2	1	-6	-15	5	15	15	6	-5
Nov	-0.2	-1	-2	-5	-8	0	2	1	-7	-16	5	15	15	5	-6
Dec	0.0	0.0	-0.1	-0.3	-1	1	6	10	12	12	6	21	27	29	28

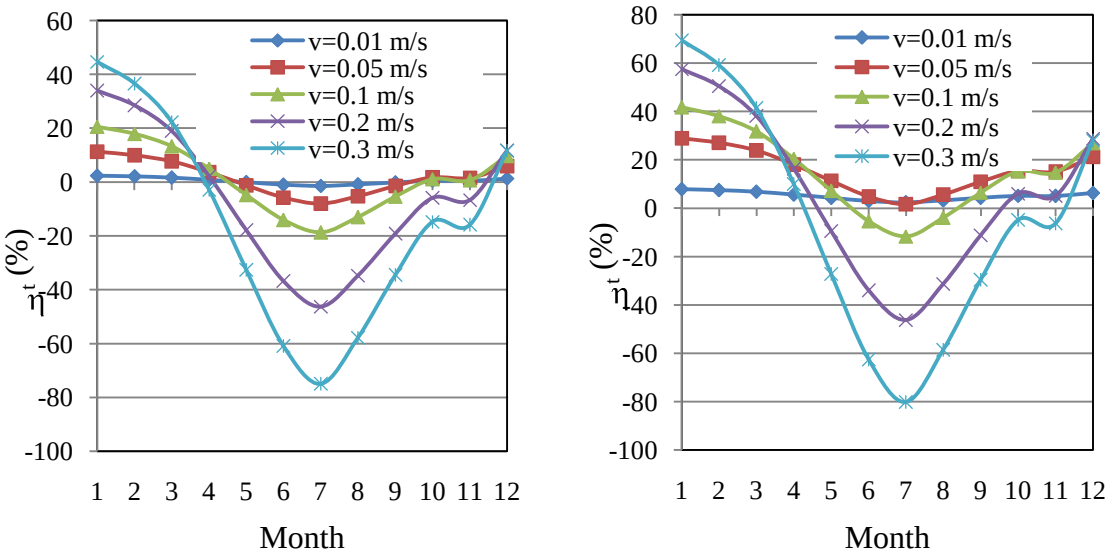

Figure 10. Variation of thermal efficiency for various air velocities in the duct. b=4m, (a) air gap depth =40mm and (b) air gap depth=80mm.

4.4.2 Effect of changing the air gap depth, *D*, at constant air velocity

Fig. 13 shows the effect of increasing air gap depth, *D*, on the thermal efficiency for a given air velocity. In winter, generally, for a given air velocity, increasing the air gap depth increased the thermal efficiency (Fig. 11). For smaller velocities and smaller air gaps (for example, up to 0.1m/s velocity and 10mm air gap depth) the thermal efficiency in winter was less than 3%. In

most cases, from April to September, the thermal efficiency was negative, meaning the outlet temperature, T_f, was lower than the ambient temperature.

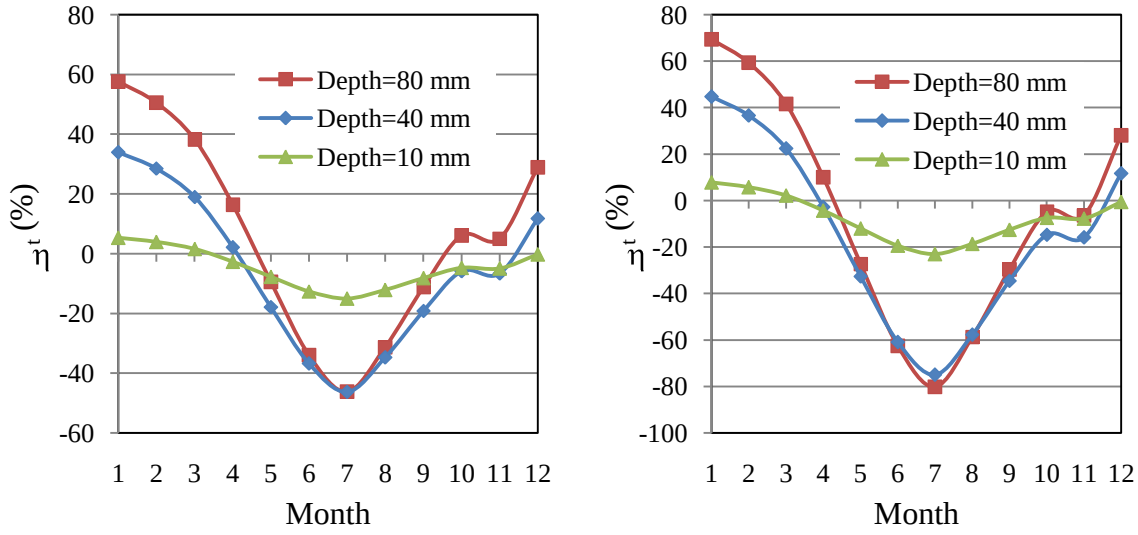

Figure 11. Variation of thermal efficiency for various air gap depths.*b*=4m, (a) *v*=0.2m/s and (b) *v*=0.3m/s

It is noted that the reduction in thermal energy in summer is desirable because space heating is not required. However, if the requirement is to recover as much thermal energy as possible throughout the year for reasons other than space heating, then the air velocity should be decreased (Table 9). For example, for 80 mm air gap depth, on average, decreasing the air velocity from 0.3 m/s to 0.1 m/s increased the thermal efficiency from -38 % to 9 %, for months from May to November. On the other hand, the PV's electrical efficiency decreased from 15% to 14% on average for those months when the air velocity is reduced from 0.3 m/s to 0.1 m/s. Numbers in bracket indicate the PV's electrical and thermal efficiency when the air velocity was 0.1 m/s.

Table 9: Optimizing the recovery of thermal energy throughout the year.

Month	Depth=80 mm		
	v (m/s)	η_{pv} (%)	*v* (m/s)
Jan		16.1	69
Feb		15.9	59
Mar		15.7	42
Apr	0.3	15.6	10
May		(15.4) 14.6	(-27) 11
Jun		(15.3) 14.5	(-63) 5
Jul		(15.1) 14.2	(-80) 2
Aug		(15.1) 14.1	(-59) 6
Sep		(15.1) 14.0	(-30) 11
Oct		(15.4) 14.3	(-5) 15
Nov	0.1	(15.4) 15.1	(-6) 15
Dec	0.3	16	28

The above results suggest that proper fan control strategies must be developed and deployed to optimize the total energy production; both thermal and electrical.

5. Conclusions

In this study, the influence of design parameters such as air flow velocity and air gap depth, *D*, between a PV panel and glass wall of photovoltaic/thermal (PV/T) curtain wall on the thermal and electrical efficiency was investigated. The most important findings are:

- Generally, the temperature ($\Delta T=T_f - T_a$) recovered is higher in winter and fall seasons. Generally, the outlet temperature decreases with increasing air flow rate,
- Both the thermal and electrical energy were found to be higher in winter and fall seasons. From May to November, higher air velocities lead to negative thermal energy recovered,
- When the PV temperature was higher than the reference temperature (25°C) their efficiency was less than the assumed efficiency (15%) at the reference temperature,
- Generally, for a given air gap, increasing the air velocity increased the PV's electrical efficiency. For larger air gaps, the increase in PV efficiency was larger,
- Generally, in winter and fall seasons, increasing the air flow velocity increased the thermal efficiency. Between May and September, increasing the air velocity reduced the thermal efficiency.

6. Nomenclature

b	width of a collector [m]	T_a	ambient temperature [°C]
C_p	specific heat capacity of air [J /kgK]	T_f	fluid (air) temperature [°C]
D	depth of the air gap [m, mm]	T_g	glass temperature [°C]
h_{cpv}	convection heat transfer coefficient, PV panel side [W/Km^2]	T_{pv}	photovoltaic (PV) panel temperature [°C]
h_{cg}	convection heat transfer coefficient, glass side [W/Km^2]	T_i	temperature inside the room [°C]
h_i	natural convection heat transfer coefficient[W/Km^2]	U_g	heat transfer resistance of the glass (R_g) and the interior heat transfer resistance between the glass and the room air ($1/h_i$) [W/Km^2]
h_{rs}	radiation heat transfer coefficient, between the PV and the sky [W/Km^2]	U_{pv}	the heat transfer resistance of the PV panel with thickness δ_{pv} and the conductivity k_{pv} and the external heat transfer resistance ($1/h_w$) *and* ($1/_{hrsky}$) [W/Km^2]
h_{rpvb}	radiation heat transfer coefficient, between the back of the PV and the glass [W/Km^2]		
h_{rgs}	radiation heat transfer coefficient, between the glass and the PV [W/Km^2]	v	velocity of air [m/s]
h_w	wind convection heat transfer coefficient [W/Km^2]	v_w	wind velocity [m/s]
I_r	solar radiation intensity incident on the surface [W/m^2]	α_{pv}	PV panel absorptance
L	height of the façade integrated PV [m]	α_g	glass absorptance
m_a	mass flow rate of air [kg/s]	η_{el}	electrical conversion efficiency of a PV panel [%]
R_g	thermal resistance of the glass [m^{2}K/W]	ρ	air density [kg/m^3]

7. References

[1] Solar Energy Perspectives: Executive Summary, International Energy Agency. 2011.
[2] Pantic, S., Candanedo, L., and Athienitis, A.K. 2010, "Modeling of energy performance of a house with three configurations of building-integrated pohotvoltaic/thermal systems", *Energy and Buildings,* Vol. 42, pp. 1779-1789.
[3] Clarke, J.A., Hand, J.W., Johnstone, C.M., Kelly, N., and Strachan, P.A. 1996, "Photovoltaic-integrated building facades", *Renewable Energy,* Vol. 8, pp. 475-479.
[4] Mei, L., Infield, D., Eicker, U., and Fux, V. 2003, "Thermal modeling of a building with an integrated ventilated PV façade", *Energy and Buildings,* Vol 35, pp. 605-617.
[5] Infield, D., Eicker, U., Fux, Mei, L., and Schumacher J. 2006, "A simplified approach to thermal performance calculation for building integrated mechanical ventilated PV facades", *Building and Environment,* Vol. 41, pp. 893-901.
[6] Infield, D., Mei, L., and Eicker, U. 2004, "Thermal performance estimation for ventilated PV façade", *Solar Energy,* Vol.76, pp. 93-98.
[7] Cartmell, B.P., Shankland, N.J., Fiala, D., HanbyV. 2004, "A multi-operational ventilated photovoltaic and solar air collector: application, simulation and initial monitoring feedback", *Solar Energy*, Vol. 76, pp. 45–53.
[8] Chow, T.T., He, W., and Ji, J. 2007, "An experimental study of façade-integrated photovoltaic/water-heating system", Applied Thermal Engineering, Vol. 27, pp. 37-45.
[9] Charron, R., and Athienitis, A. K. 2006, "Optimization of the performace of double facades with integrated photvoltaic panels and blinds", *Solar Energy*, Vol (80), pp. 482-491.
[10] Incropera, F. P., Dewitt, D. P. A. 1990, Introduction *to Heat Transfer*, John Wiley & Sons, New York.
[11] Skoplaki, E., and Palyvos, J. A. 2009, "On temperature dependence of photovoltaic module electrical performances: A review of efficiency/power correlations", *Solar energy*, Vol. 83, pp. 614- 624.
[12] Garg, H.P., Agarwal, R.K. 1995, "Some aspects of a PV/T collector/forced circulation flat plate solar water heater with solar cells", *Energy Conversion and Management*, Vol. 36, pp. 87–99.
[13] Evans, D.L., Florschuetz, L.W. 1978, "Terrestrial concentrating photovoltaic power system studies", *Solar Energy*, Vol. 20, pp. 37–43.
[14] Hachem, C., Athienitis, A., and Fazio, P. 2012, "Design of roofs for increased solar potential BIPV/T systems and their applications to housing units, *2012 ASHRAE Annual Conference*, San Antonio, Texas, USA, SA-12-02.

8. Acknowledgements

The authors gratefully acknowledge the financial support of the Natural Sciences and Engineering Research Council of Canada (NSERC), Toronto Atmospheric Fund (TAF), MITACS and Ryerson University.

9. Biography

Dr. Getu Hailu is a MITACS Elevate Postdoctoral Fellow in the Department of Mechanical and Industrial Engineering, Ryerson University. For his PhD, he developed environmentally-friendly micro-machining technique, which focused on cryogenic abrasive jet micro-machining of polymeric and elastomeric materials. He also worked in the area of design and development of water pump components for several years. He has published more than 20 refereed journal and conference papers.

Dr. Alan Fung, P.Eng. (Ontario, Nova Scotia), an Associate Professor in the Department of Mechanical and Industrial Engineering, Ryerson University, oversees a vigorous research program on sustainable building integrated energy systems/“Net Zero” energy buildings. He participates in the NSERC Smart Net-zero Energy Buildings Research Network (SNEBRN) and works closely with public and private sectors in promoting sustainable technology development. He is also the faculty adviser of Ryerson ASHRAE Student Chapter.

Mr. Peter Dash received his BSc with First Class Honours in Mechanical Engineering from Queen's University. Currently he is working on his MA Sc in Mechanical Engineering at Ryerson University. His research interests include energy conservation and renewable energy production.